常规磁共振T_2WI影像可诊断≥5 mm颅内动脉瘤

姚发明[1],邵丽敏[2],朱姬莹[3],朱庆庆[4],俞飞丹[4],吕骏晖[4],韩志江[4]
[1]广德市中医院放射科,安徽 广德 242200;[2]浙江中医药大学第四临床医学院,浙江 杭州 310053;[3]西湖大学医学院附属杭州市第一人民医院放射科,浙江 杭州 310006;[4]浙江大学医学院附属邵逸夫医院放射科,浙江 杭州 310016

摘要:目的 探讨常规磁共振T_2WI影像在≥5 mm颅内动脉瘤(IAs)诊断中的价值。**方法** 回顾性收集2019年1月~2024年12月浙江大学医学院附属邵逸夫医院151例经CT血管造影(CTA)、磁共振血管成像(MRA)或数字减影血管造影(DSA)证实且≥5 mm的IAs患者的磁共振T_2WI影像,151例患者共162枚IAs,依据诊断难度将其分为漏诊组、不确定组、确诊组,分析3组瘤体大小、位置、T_2-血管流空征等对IAs诊断的影响,并分析2位影像诊断医师观察者间一致性。**结果** 162枚IAs中,漏诊组、不确定组、确诊组分别占13.6%(22/162)、34.0%(55/162)和52.4%(85/162),确诊组瘤体大小[10.90(8.20,13.15)mm]大于不确定组[6.20(5.60,7.90)mm,*P*_corr<0.05]和漏诊组[5.55(5.18,6.55)mm,*P*_corr<0.05],不确定组和漏诊组间差异无统计学意义(*P*_corr=0.397)。IAs好发位置为大脑中动脉、颈内动脉眼段、颈内动脉交通段和椎动脉,而3组间瘤体位置分布差异无统计学意义(*P*=0.825)。完全与部分T_2-血管流空征在漏诊组、不确定组和确诊组分别占72.7%(16/22) *vs* 27.3%(6/22)、67.3%(37/55) *vs* 32.7%(18/55)和57.5%(49/85) *vs* 42.4%(36/85)(*P*=0.306)。151例患者中,发生蛛网膜下腔出血3例。2位诊断医师观测者间一致性良好(Kappa=0.890,95% *CI*:0.839~0.941,*P*<0.05)。**结论** 常规磁共振T_2WI影像在≥5 mm的IAs诊断中展示出潜在临床应用价值,对IAs的T_2WI影像特征进行准确识别,有望提升IAs诊断准确率,降低蛛网膜下腔出血等并发症。

关键词:磁共振成像;颅内动脉瘤;计算机断层扫描血管造影;磁共振血管成像;数字减影血管造影

Conventional magnetic resonance T2-weighted imaging can diagnose intracranial aneurysms ≥5 mm

YAO Faming[1], SHAO Limin[2], ZHU Jiying[3], ZHU Qingqing[4], YU Feidan[4], LÜ Junhui[4], HAN Zhijiang[4]
[1]Department of Radiology, Guangde Traditional Chinese Medicine Hospital, Guangde 242200, China; [2]The Fourth School of Clinical Medicine, Zhejiang Chinese Medical University, Hangzhou 310053, China; [3]Department of Radiology, Affiliated Hangzhou First People's Hospital, Westlake University School of Medicine, Hangzhou 310006, China; [4]Department of Radiology, Affiliated Sir Run Run Shaw Hospital, Zhejiang University School of Medicine, Hangzhou 310016, China

Abstract: Objective To evaluate the diagnostic value of conventional magnetic resonance T_2WI for intracranial aneurysms (IAs) ≥ 5 mm, aiming to reduce the rates of missed and uncertain diagnosis. **Methods** We retrospectively collected magnetic resonance T_2WI data of 151 patients with IAs ≥ 5 mm, confirmed by computed tomography angiography (CTA), magnetic resonance angiography (MRA), or digital subtraction angiography (DSA), at Sir Run Run Shaw Hospital, Zhejiang University School of Medicine, from January 2019 to December 2024. A total of 162 IAs from the 151 patients were identified and categorized into a missed-diagnosis group, an uncertain-diagnosis group, and a confirmed-diagnosis group based on diagnostic difficulty. The impacts of aneurysm size, location, and T_2-vascular flow void sign on the diagnosis of IAs were analyzed among the three groups. Additionally, the inter-observer agreement between two radiologists was evaluated. **Results** Among the 162 IAs, the proportions of the missed-diagnosis, uncertain-diagnosis, and confirmed-diagnosis groups were 13.6% (22/162), 34.0% (55/162), and 52.4% (85/162), respectively. The aneurysm size in the confirmed-diagnosis group [10.90 (8.20, 13.15) mm] was significantly larger than that in the uncertain-diagnosis group [6.20 (5.60, 7.90) mm, *P*_corr<0.05] and the missed-diagnosis group [5.55 (5.18, 6.55) mm, *P*_corr<0.05], while no significant difference was observed between the uncertain and missed diagnosis groups (*P*_corr=0.397). IAs were predominantly located in the middle cerebral artery, ophthalmic segment of the internal carotid artery, communicating segment of the internal carotid artery, and vertebral artery, with no significant difference in location distribution among the three groups (*P*=0.825). The proportions of complete versus incomplete T_2-vascular flow void sign in the missed-diagnosis, uncertain-diagnosis, and confirmed-diagnosis groups were 72.7% (16/22) *vs* 27.3% (6/22), 67.3% (37/55) *vs* 32.7% (18/55), and 57.5% (49/85) *vs* 42.4% (36/85), respectively (*P*=0.306). Among the 151 patients, subarachnoid hemorrhage occurred in 3 cases. The inter-observer agreement between the two radiologists was excellent (Kappa=0.890, 95%*CI*: 0.839~0.941, *P*<0.05). **Conclusion** Conventional magnetic resonance T_2WI demonstrates potential clinical value in the diagnosis of IAs ≥ 5 mm. Accurate identification of T_2WI features of IAs is expected to improve diagnostic accuracy and reduce complications such as subarachnoid hemorrhage.

Keywords: magnetic resonance imaging; intracranial aneurysm; computed tomography angiography; magnetic resonance angiography; digital subtraction angiography

收稿日期:2025-05-24
基金项目:浙江省自然科学基金(ZCLQN26H0901);浙江省卫生健康行业科技计划(委省共建项目)(WKJ-ZJ-26047)
作者简介:姚发明,主治医师,E-mail: 1963240060@qq.com
通信作者:韩志江,博士,副主任医师,E-mail: hzj1022@zju.edu.cn

颅内动脉瘤(IAs)是一种严重威胁人类健康的疾病,人群发病率为1.0%~5.0%[1-3],占非创伤性蛛网膜下腔出血的80%~85%[1],后者病死率高达50.0%[3]。早期发现并采取个性化诊疗方案对IAs患者极其重要。CT

血管造影(CTA)和磁共振血管成像(MRA)是评估动IAs的无创检查方法。其中对于≥3.0 mm的IAs,CTA的敏感度和特异度分别为77.0%~97.0%和87.0%~100%[1],MRA的敏感度和特异度分别为70.0%~99.0%和94.0%~100%[1, 2]。数字减影血管造影(DSA)可发现更多CTA和MRA所不能显示的微小IAs,一直被视为诊断IAs的金标准[3-5]。尽管CTA和MRA在IAs诊断方面均具有较高的敏感度和特异度,但二者并非常规CT或MRI扫描序列,多在临床医师高度怀疑IAs时才检查;DSA则常在CTA或MRA证实或高度怀疑IAs时,或针对原因不明蛛网膜下腔出血患者,为进一步治疗才使用的手段。若能在常规MRI检查中,通过IAs影像特征对其进行初步筛查,会提升无症状IAs的发现率,助力临床医师采取个性化治疗方案,降低IAs破裂风险。尽管已有研究探讨了常规MRI偶然发现脑血管病变的价值[6],并指出其对≥4 mm动脉瘤具备一定的诊断潜力[7],但现有报道多局限于典型征象的图谱式展示或整体检出率的统计,缺乏基于诊断难度的分组分析,且未深入探讨瘤体位置、T_2-血管流空征等因素对IAs诊断的影响。本文通过回顾151例患者的162枚IAs的T_2WI影像特征,旨在减少漏诊和不确定诊断的概率,降低蛛网膜下腔出血等严重并发症的发生。

1 资料与方法

1.1 一般资料

本研究回顾性收集2019年1月~2024年12月在浙江大学医学院附属邵逸夫医院经CTA、MRA或DSA证实的151例患者的162枚IAs,其中男性58例,女性93例,年龄30~93(65.1±12.4)岁。54例患者收缩压>140 mmHg,23例舒张压>90 mmHg,二者均高为13例。78例患者因头晕、头痛就诊,73例患者因肢体乏力、视力障碍、健康体检等其他原因就诊。

纳入标准:具有完整磁共振T_2WI影像;至少具备CTA、MRA或DSA检查中的1种。排除标准:IAs最大径<5.0 mm(CTA、MRA或DSA影像测量结果);T_2WI影像质量差,无法对IAs进行评估;T_2WI影像与CTA、MRA或DSA相隔时间>1年,或虽相隔时间≤1年,但IAs在T_2WI影像所测的最大径,较在CTA、MRA、DSA影像上的最大径>2.0 mm。本研究获得浙江大学医学院附属邵逸夫医院伦理委员会批准(审批号:2025-2242-01),并豁免知情同意。

1.2 检查方法

使用3.0T(GE、西门子)和1.5T(GE、西门子、联影)MRI扫描仪,TR 3910~6000 ms,TE 86~105 ms,NEX 1~1.5,FOV为210 mm×210 mm~240 mm×240 mm,矩阵为320×218~416×416,层厚5 mm,层间距1.0~1.5 mm,像素频率带宽163~280 Hz,回波链长度15~32。

1.3 分析方法

分别由工作10年的影像诊断医师A和工作20年的影像诊断医师B进行独立阅片,对意见不一致的病例,2位医师讨论后得出一致结果。依据瘤体位置、大小和T_2-血管流空征对IAs分组:漏诊组定义为借助CTA、MRA或DSA影像诊断报告中位置的描述,仍无法在T_2WI影像上确定IAs轮廓,需对照CTA、MRA或DSA影像才能确定;确诊组定义为无需CTA、MRA或DSA影像诊断报告即可确定IAs轮廓;不确定组即不符合以上两组标准,包括无需CTA、MRA或DSA影像诊断报告即可发现异常,但不能确定其轮廓,或通过CTA、MRA或DSA影像诊断报告中IAs位置描述,能确定瘤体轮廓。瘤体位置分为颈内动脉(床突段、眼段、交通段)、大脑前动脉、大脑中动脉、大脑后动脉、前交通动脉、后交通动脉、左右椎动脉、基底动脉和其他位置。依据相关指南与共识[8-11],除梭形动脉瘤测量轴位最大径外,其它IAs测量最大层面最大径。完全T_2-血管流空征定义为在T_2WI影像上,IAs呈均匀低信号,其整体信号与邻近动脉一致,与高信号的脑脊液形成鲜明对比;否则为部分T_2-血管流空征,即瘤体信号不均匀,表现为流空信号与其他信号并存;对于信号均匀的较小IAs,考虑到部分容积效应,视为完全T_2-血管流空征象[12-15]。

1.4 统计学分析

采用SPSS 27.0软件进行统计分析,非正态分布的计量资料(瘤体最大径)以中位数(上下四分位数)表示,3组间的比较采用Kruskal-Wallis检验,总体差异有统计学意义时进一步使用Dunn检验进行事后两两比较,并采用Bonferroni法对显著性水平进行校正。计数资料(瘤体的位置、T_2-血管流空征)以n(%)表示,组间比较采用卡方检验或Fisher精确检验。采用Kappa检验评估2位医师之间的一致性,Kappa≥0.75视为优秀的一致性,0.40~0.74视为尚好至中等的一致性,<0.40则视为一致性较差。以P<0.05为差异有统计学意义。

2 结果

2.1 一致性检验

医师A与医师B对162枚IAs分漏诊组、不确定组和确诊组时,观察者间一致性良好(Kappa=0.890,95% *CI*: 0.839~0.941,P<0.05,图1A)。因医师B的独立判断与共同判断结果一致性(Kappa=0.990, 95% *CI*: 0.975~1.000,P<0.05,图1C)优于医师A(Kappa=0.934, 95% *CI*: 0.896~0.972,P<0.05,图1B),后续研究均以医师B的初次独立判断作为标准。

2.2 3组IAs分布状态、大小和位置

151例162枚IAs中,单发142例142枚,双发7例14枚,三发2例6枚。

漏诊组、不确定组(图2、3)和确诊组(图4、5)分别为22枚、55枚和85枚。漏诊组、不确定组和确诊组IAs平均最大径依次增大,分别为5.55(5.18,6.55) mm、6.20(5.60,7.90) mm和10.90(8.20,13.15)mm。IAs最大径在3组间分布差异有统计学意义(P<0.05)。确诊组最

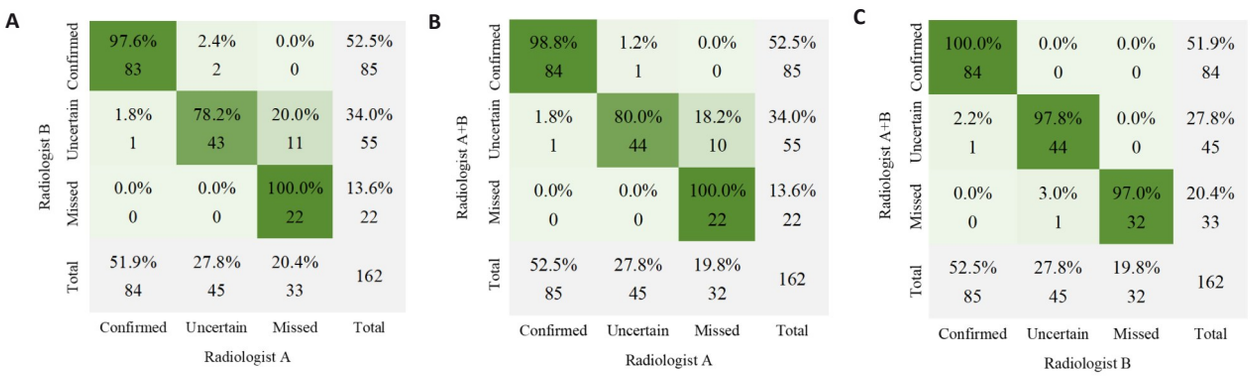

图1 医师间动脉瘤判读一致性矩阵图

Fig. 1 Inter-rater consistency matrix for aneurysm interpretation. **A**: The agreement matrix between the two physicians; **B**: The agreement matrix between Physician A and the consensus reading of the two physicians; **C**: The agreement matrix between Physician B and the consensus reading of the two physicians. Missed: Missed-diagnosis group; Uncertain: Uncertain-diagnosis group; Confirmed: Confirmed-diagnosis group.

大径高于不确定组(P_corr<0.05),其值约为不确定组的1.758倍(95% *CI*:1.593~1.941);确诊组最大径亦高于漏诊组(P_corr<0.05),其值约为漏诊组的1.964倍(95% *CI*:1.767~2.183);不确定组与漏诊组间差异无统计学意义(P_corr=0.397)。

10个瘤体位置在3组间差异无统计学意义(P=0.825),其中大脑中动脉、颈内动脉眼段和颈内动脉交通段为3组IAs好发位置,3组间差异无统计学意义(P=0.964),其中位于大脑中动脉分叉处所占比例分别为75.0%(6/8)、94.1%(16/17)、90.9%(20/22),此外椎动脉亦是确诊组瘤体好发位置之一(表1)。

2.3 3组IAs在T_2-血管流空征分布

T_2WI影像上,完全流空征象(图4)和部分流空征象(图5)的IAs在漏诊组、不确定组和确诊组中的分布差异无统计学意义(P=0.306,表2)。

2.4 IAs继发蛛网膜下腔出血或脑血肿

151例IAs患者在MRI检查1年内,3例继发蛛网膜下腔出血伴或不伴脑血肿(图3),IAs位置分别为大脑前动脉(n=1)和颈内动脉交通段(n=2)。

3 讨论

基于常规T_2WI影像对IAs进行简洁、合理的分组,能更好地总结IAs影像特点,降低漏诊率,适合大范围普及应用。本研究结果发现IAs难易程度和降低漏诊率,创新性地将IAs分为漏诊组、不确定组和确诊组,结果显示2位医师在判断确诊组时高度一致(97.6%),而在漏诊组和不确定组中,经验丰富的医师B将更多医师A认为的漏诊组病例归入到不确定组;对于不确定组患

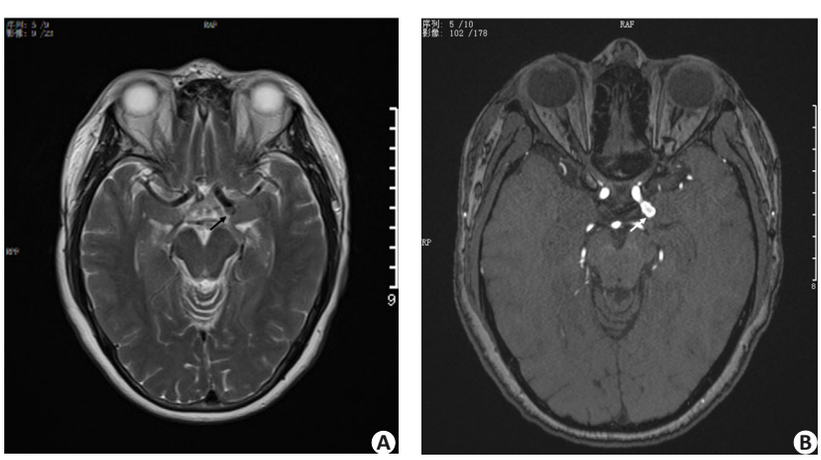

图2 患者女性, 59岁, 头晕、耳鸣1月入院

Fig. 2 A 59-year-old female patient admitted with 1-month history of dizziness and tinnitus. **A**: T_2WI demonstrates a cystic protrusion posterior to the left internal carotid artery communicating segment, showing signal intensity similar to adjacent brain parenchyma but significantly lower than neighboring vessels (black arrow). This finding was classified as missed-diagnosis group by radiologist A and uncertain-diagnosis group by radiologist B [Window width (WW) 1200; Window level (WL) 578)]. **B**: Magnetic resonance angiography (MRA) demonstrates an aneurysm at the internal carotid artery communicating segment (white arrow) (WW 550, WL 240).

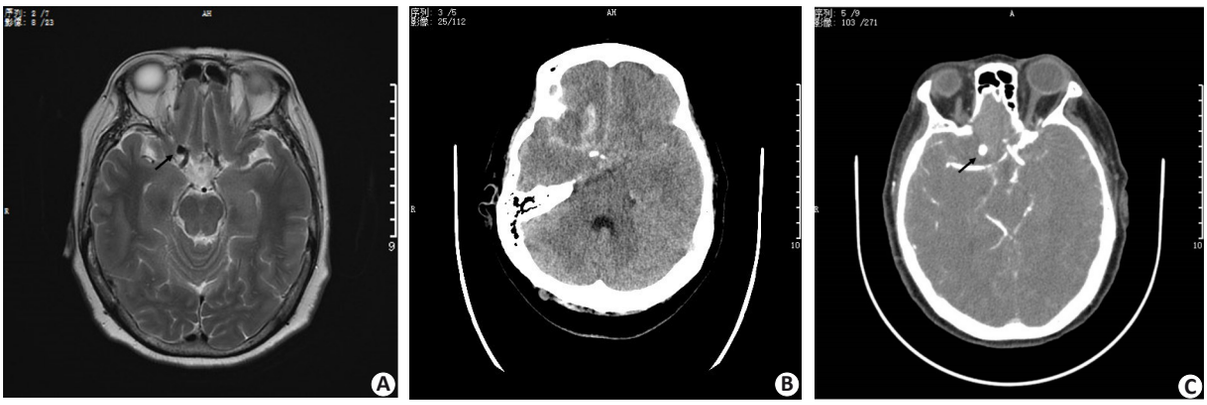

图3 患者女性, 52岁, 头痛1 h入院

Fig. 3 A 52-year-old female patient admitted with 1-hour history of headache. **A**: T_2WI shows an aneurysm at the right internal carotid artery ophthalmic segment (black arrow). Radiologist A misidentified this as tortuous internal carotid artery and categorized it as missed-diagnosis group, while radiologist B classified it as uncertain-diagnosis group (WW 1100, WL 500). **B-C**: Computed tomography angiography (CTA) confirmed the right internal carotid artery ophthalmic segment aneurysm with subarachnoid hemorrhage and right frontal lobe hematoma (black arrow). These findings were detected 30 days after the initial examination shown in Fig.3A (B: WW 80, WL 35; C: WW 480, WL 100).

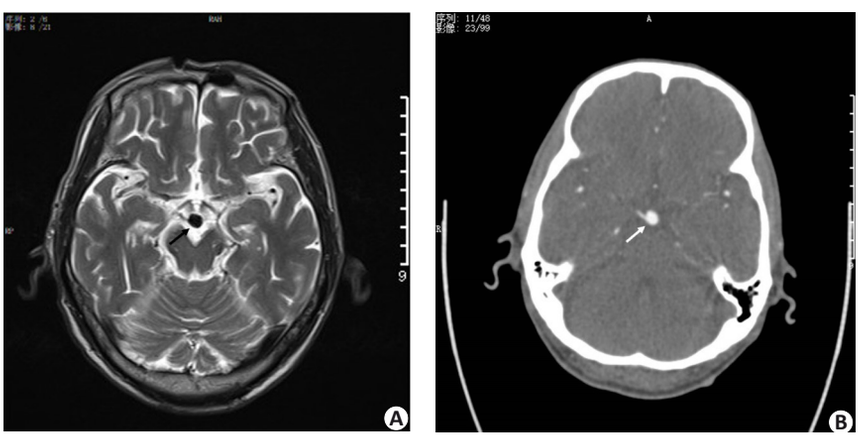

图4 患者男性, 78岁, 右侧肢体无力15 h, 加重伴口齿含糊6 h入院

Fig. 4 A 78-year-old male patient was admitted with 15-hour history of right-sided limb weakness, which worsened in the last 6 hours accompanied by slurred speech. **A**: T_2WI demonstrates complete vascular flow void signal sign of an intracranial aneurysm at the basilar artery tip (black arrow). Both radiologist A and radiologist B classified this case into the confirmed-diagnosis group (WW 1370, WL 680). **B**: CTA confirms the presence of an aneurysm at the basilar artery tip (white arrow) (WW 330, WL 70).

者,影像医师可建议MRA或CTA进一步排查。

IAs大小不同,其年增长率不同(0.53%~11.64%)[16, 17],本研究中,MRI检查与CTA、MRA、DSA间隔最长为1年,主要考虑4种检查价格均昂贵,短期内在同一医疗中心同时行MRI与其他3项中任何一项检查的患者少;另外,1年内体积增长率对于漏诊组、不确定诊断组和确定诊断组均有限,尤其是前二者。瘤体越小,越易漏诊或不确定诊断,本组资料显示,IAs确诊组最大径平均值是漏诊组的1.964倍,是不确定组的1.758倍;漏诊组和不确定组最大径平均值的差异无统计学意义,表示降低漏诊组、提高不确定组诊断比例,主要依靠临床和其他影像诊断经验。本组研究中T_2WI层厚5 mm,与国内外研究中颅脑MRI扫描层厚基本一致[18-20],部分漏诊组和不确定诊断组IAs最大径5.0 mm,无法确保扫描层面经过IAs最大层面,或多或少存在容积效应,导致IAs大小和影像学特征存在一定差异,甚至漏诊,如某患者瘤体为5.1 mm,稍大于层厚,内部存在容积效应,易与周围脑实质混淆,故经验不足的医师A将其归入漏诊组;扫描层厚越薄,所能获得的影像信息越充分,漏诊和不确定诊断率越低,但扫描层厚变薄会导致整体扫描时间延长,如何兼顾二者需要结合临床需求进行。本组资料中,漏诊组和不确定组常见的瘤体位置依次是大脑中动脉分叉处、颈内动脉眼段和颈内动脉交通段,考虑与以下因素相关:这些位置是IAs好发部位[8];大脑中动脉分叉处较小IAs易误认为是大脑中动脉末端,并非是瘤样突起,而基底动脉尖部向上突起的

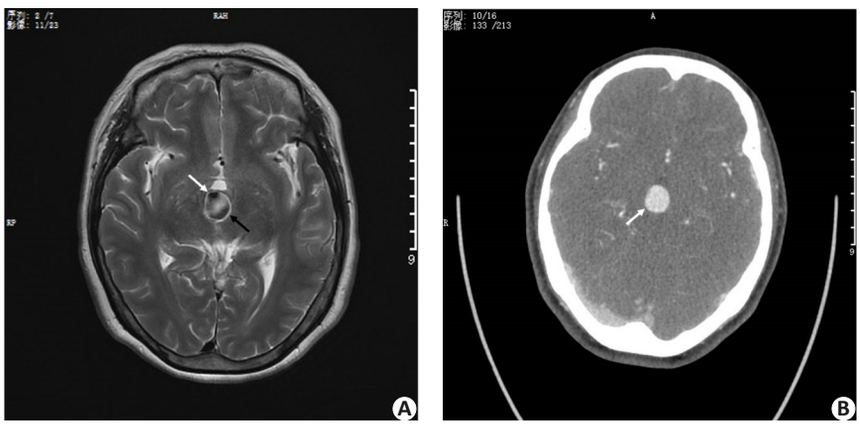

图5 患者, 女性, 58岁, 头痛5月入院

Fig. 5 A 58-year-old female patient admitted with a 5-month history of headache. **A**: T_2WI demonstrates faint patchy hyperintensity and partial vascular flow void sign caused by blood turbulence within the basilar tip aneurysm (white arrow), along with a circumferential cerebrospinal fluid-like hyperintense rim surrounding the aneurysm (black arrow). Both radiologist A and radiologist B classified this case into the confirmed-diagnosis group (WW 940, WL 400). **B**: CTA confirms the presence of an aneurysm at the basilar artery tip (white arrow) (WW 700, WL 80).

表1 3组IAs位置分布(枚)

Tab. 1 Distribution of intracranial aneurysm locations among the three groups (n)

Location of IA	Missed-diagnosis group	Uncertain-diagnosis group	Confirmed-diagnosis group	Total
ACA	2	3	5	10
MCA	8	17	22	47
PCA	0	0	2	2
ICA-C6	4	10	14	28
ICA-C7	3	9	15	27
ACoA	2	4	1	7
PCoA	0	2	2	4
BA	1	5	6	12
VA	2	5	16	23
OA	0	0	2	2
Total	22	55	85	162

ACA: Anterior cerebral artery; MCA: Middle cerebral artery; PCA: Posterior cerebral artery; ICA-C6: Ophthalmic segment of internal carotid artery; ICA-C7: Communicating segment of internal carotid artery; ACoA: Anterior communicating artery; PCoA: Posterior communicating artery; BA: Basilar artery; VA: Vertebral artery; OA: Other arteries.

表2 3组T_2-血管流空征分布

Tab. 2 Distribution of the T_2-vascular flow void sign among the three groups (n)

Diagnostic group	Complete T_2-vascular flow void sign	Incomplete T_2-vascular flow void sign	χ^2	P
Missed-diagnosis group	16	6		
Uncertain-diagnosis group	37	18	2.368	0.306
Confirmed-diagnosis group	49	36		

The complete T_2-vascular flow void sign refers to IAs that demonstrate a homogeneous hypointense signal on T_2WI, with an overall signal intensity matching the adjacent artery (Fig. 4). The incomplete T_2-vascular flow void sign is characterized by heterogeneous signal intensity within the aneurysm (Fig.5).

IAs同样会被误认为正常基底动脉的延续;颈内动脉眼段和交通段易误认为正常颈内动脉的横断面或迂曲增粗的颈内动脉,尤其是动脉粥样硬化显著的老年患者,瘤腔周围存在附壁血栓,使瘤体信号变得更加复杂,其形成体积效应易导致小动脉瘤漏诊[12];影像诊断医师与临床医师习惯性观察脑实质结构与病变,易忽视走行于脑叶或脑裂间主要动脉及其所发生的IAs,或即使发现IAs,亦可能被误认为正常血管的流空现象。一旦IAs体积较大,能在多个层面显示,能提供更多的影像信息,漏诊概率亦会明显降低,本研究中2位医师对确诊组IAs高度一致性即说明了这点。

本研究中,尽管漏诊组、不确定组和确诊组在完全T_2-血管流空征显示方面的差异无统计学意义,但三者发生比例分别为72.7%、67.3%、57.6%,提示较大IAs在完全T_2-血管流空征显示方面有低于其他组的趋势,考虑其主要原因除了与较大瘤体更容易出现涡流外,尚与较大瘤体内易形成附壁血栓和瘤体内出血有关,从而导致瘤体内信号不均[20]。T_2-血管流空征机制为流动的血液在扫描层面内停留时间过短,未充分接受射频脉冲激励即流出层面,导致信号丢失,T_2WI呈低信号,但由于部分瘤体慢血流或涡流的缘故,T_2WI表现为等或高信号,减小IAs与周围结构信号差异[12],易导致较小瘤体漏诊和不确定诊断;而对于较大瘤体影响则有限,即使无法单独通过T_2WI影像确诊IAs,但可发现瘤体的存在,再进一步结合其他常规序列,甚至增强检查而明确诊

断。本文151例IAs患者中，在MRI检查后1年内，3例发生了蛛网膜下腔出血伴或不伴脑内血肿，发生比例为2%，低于既往研究报道[2, 3]。若在临床工作中，对行颅脑MRI检查的患者通过T_2WI影像对IAs好发位置的血管进行充分评估，筛选出可疑IAs并进一步医疗干预，将在一定程度上降低蛛网膜下腔出血等并发症的发生率。随着深度学习和AI自动检测技术的迅速发展，已有多篇基于MRA的深度学习模型实现IAs自动分割和破裂风险评估方面的相关报道[21-25]，若能构建基于常规MRI的IAs人工智能模型，并将其植入到日常工作的PACS中，能降低观察者主观经验影响，实现AI初步筛查、医师最终确定双判断模式，受益群体将更广泛[26]。

本研究的局限性在于：本研究为单中心回顾性分析，需多中心、前瞻性研究进一步验证；T_1WI序列、脂肪抑制T_2WI序列、FLAIR序列，甚至弥散加权成像序列亦是大部分医疗中心常规序列，尽管单序列应用诊断IAs价值低于T_2WI，但可作为部分或无T_2-血管流空征IAs的有效补充，后续将对此进一步联合研究；医疗中心常规颅脑MRI的T_2WI序列层厚为5 mm，为避免部分容积效应影响[27]，未纳入<5 mm的IAs；且层厚、容积效应、老年动脉粥样硬化3个因素并非独立因素，大部分为2或3个因素同时存在，难以对其中单一因素进行详细解析。

综上，常规磁共振T_2WI影像对≥ 5 mm的IAs展示出潜在应用价值，对于重点人群IAs好发部位进行常规评估，有望降低漏诊率和不确定诊断率，减少蛛网膜下腔出血等严重并发症的发生。

参考文献：

[1] Ajiboye N, Chalouhi N, Starke RM, et al. Unruptured cerebral aneurysms: evaluation and management[J]. Sci World J, 2015, 2015: 954954.

[2] Zhu CY, Liu RH, Ye YF, et al. Review article imaging evaluation for the size of saccular intracranial aneurysm[J]. World Neurosurg, 2024, 183: 172-9.

[3] Hu B, Shi Z, Lu L, et al. A deep-learning model for intracranial aneurysm detection on CT angiography images in China: a stepwise, multicentre, early-stage clinical validation study[J]. Lancet Digit Health, 2024, 6(4): e261-71.

[4] Philipp LR, McCracken DJ, McCracken CE, et al. Comparison between CTA and digital subtraction angiography in the diagnosis of ruptured aneurysms[J]. Neurosurgery, 2017, 80(5): 769-77.

[5] Brown RD, Broderick JP. Unruptured intracranial aneurysms: epidemiology, natural history, management options, and familial screening[J]. Lancet Neurol, 2014, 13(4): 393-404.

[6] Khurana NKR, Raz E, Mohamed AWH, et al. Intracranial cerebrovascular lesions on T2-weighted magnetic resonance imaging [J]. J Clin Imaging Sci, 2024, 14: 19.

[7] Caliskan E, Pekcevik Y, Kaya A. Can we evaluate cranial aneurysms on conventional brain magnetic resonance imaging?[J]. J Neurosci Rural Pract, 2016, 7(1): 83-6.

[8] Zheng YT, Xu F, Ren JM, et al. Assessment of intracranial aneurysm rupture based on morphology parameters and anatomical locations [J]. J NeuroInterv Surg, 2016, 8(12): 1240-6.

[9] 张彤宇, 刘 鹏, 向思诗, 等. 中国颅内破裂动脉瘤诊疗指南2021[J]. 中国脑血管病杂志, 2021, 18(8): 546-74.

[10] 中国女医师协会医学影像专委会, 中国脑动脉瘤智能影像诊治评估协作组. 颅内囊状未破裂动脉瘤MRI影像标注专家共识[J]. 国际医学放射学杂志, 2022, 45(4): 373-9.

[11] 中国医师协会神经介入专业委员会中国颅内动脉瘤计划研究组, 张鸿祺, 杨新健, 等. 颅内动脉瘤影像学判读中国指南(2024版)[J]. 中华神经外科杂志, 2024, 40(8): 757-73.

[12] 石士奎, 季立平, 周育夫. 颅内动脉瘤的MR诊断[J]. 医学影像学杂志, 2010, 20(11): 1586-8.

[13] 张 勇, 程敬亮, 任翠萍, 等. 颅内动脉瘤流动伪影在不同MRI序列上的表现差异[J]. 实用放射学杂志, 2008, 24(2): 148-50, 224.

[14] Zimny A, Neska-Matuszewska M, Bladowska J, et al. Intracranial lesions with low signal intensity on T2-weighted MR images-review of pathologies[J]. Pol J Radiol, 2015, 80: 40-50.

[15] Carpentieri-Primo P, Nahoum L, Almeida L, et al. The dark side of T2: central nervous system lesions with low signal intensity on T2-weighted imaging[J]. Radiol Bras, 2024, 57: e20230085en.

[16] Malhotra A, Wu X, Forman HP, et al. Growth and rupture risk of small unruptured intracranial aneurysms: a systematic review[J]. Ann Intern Med, 2017, 167(1): 26-33.

[17] Backes D, Rinkel GJE, Laban KG, et al. Patient- and aneurysm-specific risk factors for intracranial aneurysm growth: a systematic review and meta-analysis[J]. Stroke, 2016, 47(4): 951-7.

[18] Teodorescu B, Gilberg L, Koç AM, et al. Advancements in opportunistic intracranial aneurysm screening: The impact of a deep learning algorithm on radiologists' analysis of T2-weighted cranial MRI[J]. J Stroke Cerebrovasc Dis, 2024, 33(12): 108014.

[19] 张 恒, 马长江, 李 璐, 等. CT与MR诊断颅内动脉瘤敏感性和特异性对比[J]. 现代医用影像学, 2017, 26(3): 650-2.

[20] Teng MM, Nasir Qadri SM, Luo CB, et al. MR imaging of giant intracranial aneurysm[J]. J Clin Neurosci, 2003, 10(4): 460-4.

[21] Ueda D, Yamamoto A, Nishimori M, et al. Deep learning for MR angiography: automated detection of cerebral aneurysms[J]. Radiology, 2019, 290(1): 187-94.

[22] Lehnen NC, Haase R, Schmeel FC, et al. Automated detection of cerebral aneurysms on TOF-MRA using a deep learning approach: an external validation study[J]. AJNR Am J Neuroradiol, 2022, 43 (12): 1700-5.

[23] Geng C, Bao YF, Zhang JJ, et al. Automated unruptured cerebral aneurysms detection in TOF MR angiography images using dual-channel SE-3D UNet: a multi-center research[J]. Eur Radiol, 2023, 33(5): 3532-43.

[24] Joo B, Ahn SS, Yoon PH, et al. A deep learning algorithm may *Automate* intracranial aneurysm detection on MR angiography with high diagnostic performance[J]. Eur Radiol, 2020, 30(11): 5785-93.

[25] Ishihara M, Shiiba M, Maruno H, et al. Detection of intracranial aneurysms using deep learning-based CAD system: usefulness of the scores of CNN's final layer for distinguishing between aneurysm and infundibular dilatation[J]. Jpn J Radiol, 2023, 41(2): 131-41.

[26] Lewin J, Schoenherr S, Seebass M, et al. PACS-integrated machine learning breast density classifier: clinical validation[J]. Clin Imaging, 2023, 101: 200-5.

[27] Bouillot P, Delattre BMA, Brina O, et al. 3D phase contrast MRI: Partial volume correction for robust blood flow quantification in small intracranial vessels[J]. Magn Reson Med, 2018, 79(1): 129-40.

（编辑：熊一凡）